Assessment of advanced process configurations for improving workpiece surface finish in point grinding

Medina Aguirre, Fernanda; Soriano Gonzalez, Luis; Hood, Richard; Kong, Ming Chu; Novovic, Donka; Soo, Sein Leung

DOI:
10.1016/j.cirp.2023.04.078

CIRP Annals - Manufacturing Technology 00 (2023) 1–6

Contents lists available at ScienceDirect

CIRP Annals - Manufacturing Technology

journal homepage: https://www.editorialmanager.com/CIRP/default.aspx

Assessment of advanced process configurations for improving workpiece surface finish in point grinding

Fernanda Medina Aguirre[a], Luis Soriano Gonzalez[a], Richard Hood (2)[a,*], Ming Chu Kong[a], Donka Novovic (3)[a,b], Sein Leung Soo (1)[a]

[a] Machining Research Group, Department of Mechanical Engineering, School of Engineering, University of Birmingham, Edgbaston, Birmingham B15 2TT, United Kingdom
[b] Manufacturing Technology, Rolls-Royce plc, More Lane, Derby DE24 8BJ, United Kingdom

ARTICLE INFO

Article history:
Available online xxx

Keywords:
Grinding
Ultrasonic
Wear

ABSTRACT

The effect of workpiece tilt angle (0°, 30°) and tool ultrasonic vibration was evaluated when machining hardened steel with electroplated CBN grinding points (B15, B30, B54). Workpiece inclination had the greatest influence in decreasing surface roughness (Ra) by up to ~44%, with the lowest value (~0.32 µm) achieved at 30° tilt angle when ultrasonic assisted grinding using B30 wheels. Despite also reducing roughness, use of ultrasonic actuation generally increased specific volumetric grit loss (~11%) and normal forces (~14%) compared to conventional grinding when employing B15 and B30 points. No substantial microhardness modification was evident in most of the ground surfaces.

1. Introduction

Point grinding is a term that refers to the process of abrasive machining using small diameter (generally ≤ 15 mm) electroplated superabrasive wheels (also commonly known as grinding points/pins) typically mounted on a high-speed machining centre [1,2]. While grinding points have traditionally been used for post processing operations such as deburring and edge finishing/radiusing, the technology has in recent years been developed and adapted by the aerospace industry for multi-axis machining of components with geometrically complex features (airfoils, impellers, rotors) requiring high dimensional accuracy, which are not achievable using conventional large diameter grinding wheels [3,4]. Point grinding as an alternative to broaching for machining of re-entrant blade root mounting slots on turbine discs has also been evaluated. Initial feasibility studies by Burrows et al. [5,6] and Dewes et al. [7] using 15 mm diameter cylindrical grinding points for machining Inconel 718 and Udimet 720 nickel-based superalloys reported relatively low tangential (20–30 N) and normal forces (60–80 N) with no signs of significant subsurface microstructural deformation, despite a moderate reduction in microhardness near the ground surface. More importantly, compressive residual stresses were prevalent in all of the machined surfaces assessed, with maximum values of up to −600 MPa and −1350 MPa for Inconel 718 and Udimet 720 respectively [7]. This favourable residual stress regime was instrumental in the superior fatigue performance exhibited by point ground specimens over corresponding high-speed milled surfaces, which had tensile residual stresses of up to ~520 MPa [8]. Subsequent work was carried out using fir-tree profiled grinding points, with results recommending cubic boron nitride (CBN) abrasive (over diamond) and higher cutting speeds for reducing tool wear rates [9].

Although still comparatively scarce, there has been increasing interest and publications relating to point grinding of ferrous based alloys, including steels in the hardened condition. The effect of grit size (US-mesh 60, 80, 230) following face grinding of slot bases in FC200 cast iron using electroplated cup CBN points was investigated by Yan et al. [10]. No significant variation in surface roughness (Rz) was observed regardless of grit size, which was attributed to similar levels of active cutting edges on the tools. When machining a tool steel (37 ± 2 HRC) with metal bonded B64 grinding points, Uhlmann et al. [11] demonstrated that a ~50% decrease in surface roughness was obtained when a tool lead angle of 30° was employed. The performance of electroplated CBN grinding points with different grit sizes (B76, B46, B32) when machining hardened D2 steel (62 HRC) was assessed by Hood et al. [4]. Lowest surface roughness (0.8 µm Ra) and highest tool life (G-ratio of 2441) was seen when grinding with B32 tools, while uniformity of wear distribution and the number of effective cutting grains (rather than variation in operating parameters) were the primary factors affecting surface roughness. More recently, a methodology to determine the wear condition of CBN grinding points (126 μm nominal grain size) by monitoring the evolution of tool surface topography/texture using 3D imaging techniques when machining hardened D2 tool steel (60 HRC) was developed by Pietrow et al. [12]. It was determined that average surface height (S_a), skewness (S_{sk}), root mean square gradient (S_{dq}), developed interfacial area ratio (S_{dr}), reduced peak height (S_{pk}), and peak material volume (V_{mp}) parameters displayed the best correlation to grit wear progression over the duration of the trials (520 mm^3 of material removed). Analysis of surface texture parameters were

* Corresponding author.
E-mail address: R.Hood@bham.ac.uk (R. Hood (2)).

https://doi.org/10.1016/j.cirp.2023.04.078

also appropriately adjusted to account for the different wear mechanisms and presence of defects on the grinding points.

The work outlined here aimed to evaluate the influence of different process configurations involving ultrasonic tool vibration and workpiece inclination (applied individually and in combination) on resultant workpiece surface integrity, tool wear and cutting forces when point grinding using electroplated CBN wheels having varying grit sizes.

2. Experimental work

A hardened D2 tool steel (62 ± 1 HRC) was employed as the workpiece material, which were suitably prepared into rectangular shaped samples measuring 75 × 25 × 5 mm. Plain, cylindrical electroplated CBN grinding points with three different grit sizes (B54, B30 and B15) representative of finishing/fine finishing operations were assessed. All tools had a diameter of 4 mm and electroplated length of 7 mm, with tungsten carbide (WC) shanks for superior stiffness and dimensional tolerance/lower tool runout. The point grinding trials were undertaken on a DMG-Mori Ultrasonic 20 linear 5-axis high speed machining centre, with a maximum spindle rotational speed of 42,000 rpm and integrated axial ultrasonic (US) vibration capability of the tool. The grinding points were held using HSK-E32/ER11 ultrasonic toolholders at an overhang of 28 mm, which provided consistent spindle-toolholder-grinding point runout measured at < 5 µm. A bespoke fixture was utilised to secure the workpiece blocks in place, which was then clamped onto a piezoelectric three component Kistler 9257A platform dynamometer connected to 3 single channel Kistler 5011 charge amplifiers for cutting force measurement, see experimental setup in Fig. 1a. The recorded force signals were post processed using Dynoware software to obtain root mean square (RMS) values, with a low pass filter specified at a cut-off frequency of 3.5 kHz to attenuate signals approaching/above the resonance frequency of the dynamometer (> 4.0 kHz). Trials were performed wet using Hocut 795 B-EU water based emulsion (10% oil concentration) supplied via external nozzles at a flow rate of ~17 l/min.

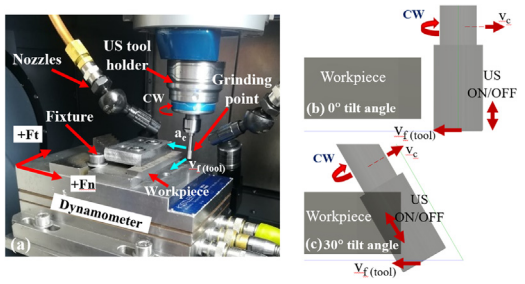

Fig. 1. (a) Experimental setup; schematic of process configuration at workpiece tilt angle of (b) 0°; (c) 30°.

Plunge grinding experiments (in down grinding mode) comprising varying abrasive size, workpiece tilt angle and tool ultrasonic actuation were carried out based on a full factorial design (total of 12 tests) with the factor levels detailed in Table 1. Schematics of the process configuration at workpiece tilt angles of 0° and 30° are shown in Fig. 1b and 1c respectively. Operating parameters held constant included radial depth of cut (a_e) of 20 µm per pass, feed rate (v_f) of 250 mm/min and tool rotational speed of 40,000 rpm leading to a peripheral cutting speed (v_c) of ~8.4 m/s, which were based on conditions employed in previous related work [4]. For trials incorporating ultrasonic actuation (US ON), the resonant frequency of the system (spindle-toolholder-grinding point) was determined prior to test commencement by measuring the vibration amplitude over a range of ultrasonic frequencies using a high-accuracy (± 0.5 µm) Renishaw NC4 non-contact laser tool setting system. The resonant frequency was found to be 31,900 Hz, corresponding to a maximum amplitude of 1.6 ± 0.5 µm. The end of test criterion for the different grit sizes was established through a preliminary trial involving a B30 grinding point that was tested to failure. Complete removal of the nickel electroplated layer together with substrate damage was observed over significant regions of the tool after grinding 2100 mm^3 of workpiece material. This result was used as a baseline to estimate the test cessation criterion (before tool failure occurs) in terms of volume of material ground for each grit size, see Table 2.

Table 1
Experimental variables and levels.

Variable factor	Level 1	Level 2	Level 3
Abrasive grit size	B54	B30	B15
Workpiece tilt angle	0°	30°	
Tool ultrasonic actuation	US OFF	US ON	

Table 2
End of test criterion relative to tool grit size.

Tool grit size	End of test criterion based on volume ground (mm^3)
B54	4350 (~twice the failure baseline of B30 tool)
B30	1875 (11% below the failure baseline of B30 tool)
B15	1238 (41% below the failure baseline of B30 tool)

Surface topography of the grinding points were characterised prior to the start and following the end of each trial using the technique described in a previous publication [4]. Several regions (each over an area of 4.0 × 0.814 mm) around the tool periphery were scanned with an Alicona G5 InfiniteFocus optical microscope to produce bearing ratio curves and determine the S_{pk} texture parameter, which provide an indication of the grinding point structure/grit density and average grain protrusion respectively. Grinding point wear is commonly evaluated via wheel diametric measurements [1,4,9], however it is generally difficult to precisely capture the relatively small geometric variations due to abrasive wear using this approach, particularly for fine grained tools. Therefore, a customised method utilising the bearing ratio curves was developed for tool wear estimation by determining the volume of grit loss per unit area after each grinding test. Fig. 2 illustrates the methodology/procedure implemented. The bearing ratio curves above the mean plane (0 µm height) represents the distribution of grit material protruding above the bond. Curves corresponding to the new and worn condition (measured at equivalent sections of the tool) were initially compared on the same plot as shown in Fig. 2a. Considering that a rise in the percentage of grit material cannot occur as wear progresses, bearing curves relating to the worn tools were adjusted accordingly to intersect curves in the new condition at the mean plane (Fig. 2b). The area between the new and adjusted worn bearing curves (above the mean plane) representing the volume loss of grit material per unit area, was then calculated, see Fig. 2c. The total volume loss of abrasive was subsequently estimated by multiplying the calculated values with the lateral area of the tool grinding surface (height of 5 mm and tool diameter of 4 mm).

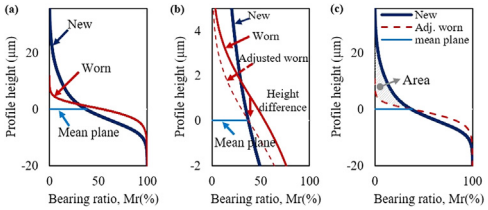

Fig. 2. Procedure for specific volume of grit loss estimation: (a) Comparison of bearing ratio curves for new and worn tools; (b) height adjustment of curve for worn tools; (c) calculation of area between curves.

Workpiece surface roughness (Ra and Rz) was measured parallel and perpendicular to the feed direction using a portable profilometer initially after every 5 passes until 65 tool passes, followed by intervals of 20, 40 and 100 passes for the B15, B30 and B54 grinding points respectively. Each measurement was based on an average of 9 readings taken at different locations along the ground workpiece, with cut-off and evaluation lengths of 0.8 mm and 4.0 mm respectively, in accordance with ISO 4288 standards. Micrographs and contour plots of ground surfaces were obtained using the Alicona microscope. Selected machined surfaces were cross-sectioned parallel and perpendicular to the feed direction using wire electrical discharge machining with specimens hot mounted in bakelite followed by

Please cite this article as: F. Medina Aguirre et al., Assessment of advanced process configurations for improving workpiece surface finish in point grinding, CIRP Annals - Manufacturing Technology (2023), https://doi.org/10.1016/j.cirp.2023.04.078

grinding and polishing. Subsurface workpiece microhardness was subsequently evaluated on the cross-sectioned samples using a Mitutoyo HM-124 microhardness tester having a Knoop indenter at a load of 50 g over a duration of 15 s (based on ISO 4545–1), with 4 measurements performed at each depth level of 20, 40, 70, 100 and 200 µm beneath the ground surface.

3. Results and discussion

3.1. Grinding point surface topography characterisation

Surface topographies of the 3 different grit size tools in the as supplied/new condition are described by the bearing ratio curves and optical micrographs shown in Fig. 3, together with their respective S_{pk}, A_p (average projected grit area) and d_e (equivalent grit diameter) values. The B15 and B30 tools were found to have comparable bearing ratio curves, average equivalent grit diameter (~23 µm) and mean grain protrusion (~9 µm vs. 8 µm S_{pk}). Nevertheless, minor differences were noted with the B15 wheel surfaces exhibiting a slightly more open structure (relatively steeper bearing curve gradient), where 5% of the grits showed greater peak heights of up to 28 µm, when compared to the B30 tools (peaks up to 22 µm). Conversely, the highest peaks of up to ~39 µm were observed in the B54 grinding points as anticipated, in addition to a more open wheel structure/lower grit density than the B15 and B30 tools. Similarly, the average equivalent grit diameter (~34 µm) and S_{pk} (~17 µm) was ~48% and 89%/113% higher than the B30/B15 tools respectively.

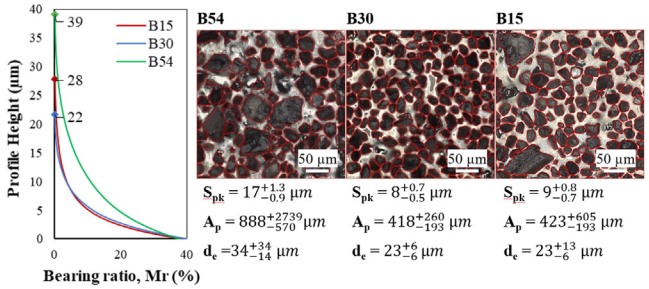

Fig. 3. Bearing ratio curves and micrographs of tool surface topographies in the new condition.

3.2. Tool wear

The calculated grit volume per unit area of the grinding points in the new and worn condition for each trial is shown in Fig. 4. It was observed that both the new B30 and B15 tools exhibited comparable specific grit volumes (~155 × 10^4 µm^3/mm^2) while the new B54 wheels typically had almost twice the volume of abrasives (~300 × 10^4 µm^3/mm^2). The results indicated that the percentage volume of grit loss at test cessation varied between 43% and 77%, with the higher volumetric losses corresponding to the coarser grained tools. In general, the variation in workpiece tilt angle (0° and 30°) appeared to have a negligible effect on tool wear, while the application of ultrasonic vibration (US ON) was found to cause marginally increased grit loss (up to ~11% higher) compared to conventional operation (US OFF), especially for the B30 and B15 grinding points. The high frequency tool oscillation during ultrasonic vibration assisted grinding (UVAG) increased the rate of grain-workpiece interaction, which likely promoted greater mechanical impact on the abrasives (hammering and rubbing of the grains), thus accelerating tool wear.

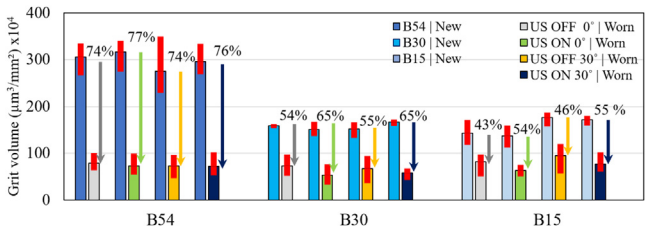

Fig. 4. Specific grit volume on tools in new and worn condition.

Associated tool G-ratios following machining with and without ultrasonic vibration at 0° workpiece tilt is detailed in Fig. 5. The B30 tool displayed the highest G-ratio of 34,810 when conventional grinding without ultrasonic actuation, which was an improvement of 9% and 14% over the B15 and B54 wheels respectively. This was attributed to the more compact wheel structure/higher grit density in the former, with similar trends previously reported by Hood et al. [4]. Application of ultrasonic vibration however led to a decline in G-ratios for all cases, with the smaller B30 and B15 grits exhibiting greater reductions of 12% and 16% respectively, in line with the increased volumetric grit loss highlighted previously. The S_{pk} values indicating mean grain protrusion/height of grinding points in the new and worn condition for each trial are presented in Fig. 6. In general, tests employing UVAG resulted in a greater decrease of S_{pk} values (between new and worn condition) for the B30 and B15 wheels in the region of ~82%, as opposed to a drop of ~73% under conventional grinding mode. In contrast, the reduction in average grain height of B54 tools following machining was largely consistent at ~87%, irrespective of process configuration. In addition, the maximum variation of measured S_{pk} values for all worn grinding points did not exceed ~2 µm, suggesting balanced wear distribution due to low tool runout.

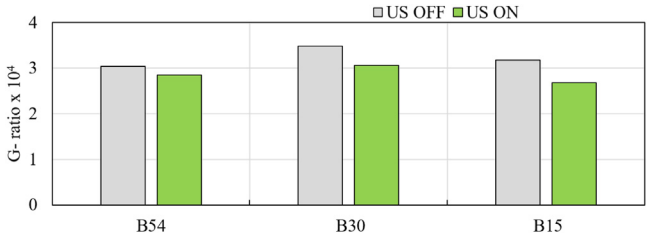

Fig. 5. Effect of ultrasonic vibration on tool G-ratio (0° workpiece tilt).

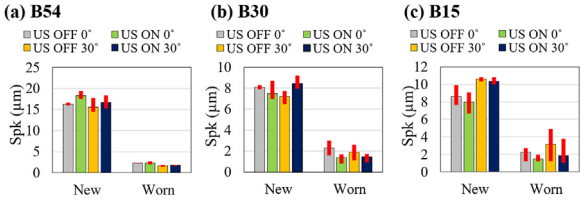

Fig. 6. Mean grain height of the grinding points in new and worn condition: (a) B54; (b) B30; (c) B15.

Fig. 7 shows sample contour plots together with associated optical micrographs of new and worn B54 tool surfaces under the various test conditions. The principal wear type observed was grain flattening/wear flat formation due to an attritious wear mechanism, which was present on all tools regardless of the experimental parameters.

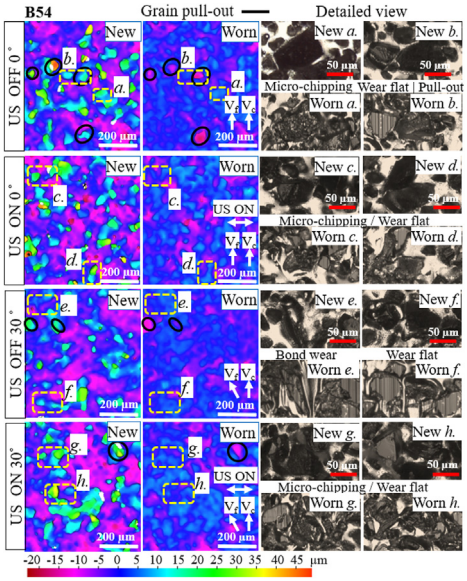

Fig. 7. Contour plots and micrographs of B54 grinding points in new and worn condition.

Please cite this article as: F. Medina Aguirre et al., Assessment of advanced process configurations for improving workpiece surface finish in point grinding, CIRP Annals - Manufacturing Technology (2023), https://doi.org/10.1016/j.cirp.2023.04.078

Signs of grit pull out and micro chipping were also evident albeit to a lesser degree, as well as instances of damage extending to the electroplated bond layer in some of the tools. Similar wear patterns/modes were also detected on the B30 and B15 grinding points.

3.3. Cutting forces

The evolution of specific grinding force components (force per unit grinding contact length) against volume of material ground for all tests are shown in Fig. 8. Specific normal forces ($F_{n'}$) when UVAG with the B30 and B15 tools were found to be ~14% higher than corresponding experiments without ultrasonic vibration. In contrast, recorded $F_{n'}$ of the B54 grinding points when operating with ultrasonic actuation were up to 20% lower than machining in conventional mode. The influence of ultrasonic vibration in reducing normal grinding forces for the B54 wheels became more pronounced as trials progressed beyond ~2000 mm^3 of material removed. The divergence in $F_{n'}$ trends between the B54 and B30/B15 tools when utilising UVAG was possibly due in part to differences in the wheel topographies/characteristics. The ultrasonic oscillations were thought to have aided penetration of the larger B54 grains into the workpiece as well as improve chip flow due to the more open structure of the grinding points. Conversely, the considerably higher grit density of the smaller grained B30/B15 tools (space between grains was approximately half of the B54 wheels) was more susceptible to wheel loading and was likely exacerbated by the ultrasonic actuation, thus resulting in the increased $F_{n'}$ observed. The elevated forces generated by the B30 and B15 grinding points when UVAG also explains the greater tool wear levels detected when compared to conventional grinding as outlined in the preceding section.

Unlike the normal force component, there was generally no major difference in specific tangential forces ($F_{t'}$) between trials performed with and without ultrasonic assistance. The only exceptions were tests involving the B54 tool with the workpiece horizontal (0°), where relatively higher $F_{t'}$ of up to ~65% was obtained when operating with UVAG. This was partially attributed to US oscillations causing increasing frictional contact between the worn grits/larger wear flats and workpiece as the trial progressed ($F_{t'}/F_{n'}$ ratio increased by two-fold). In general, the specific normal force (N/mm) was ~23% lower when machining at a 30° angle, irrespective of grit size. However, this configuration corresponded to an extended grinding point contact length of 17%, suggesting that variation in workpiece tilt angle had no major effect on total normal grinding forces (N).

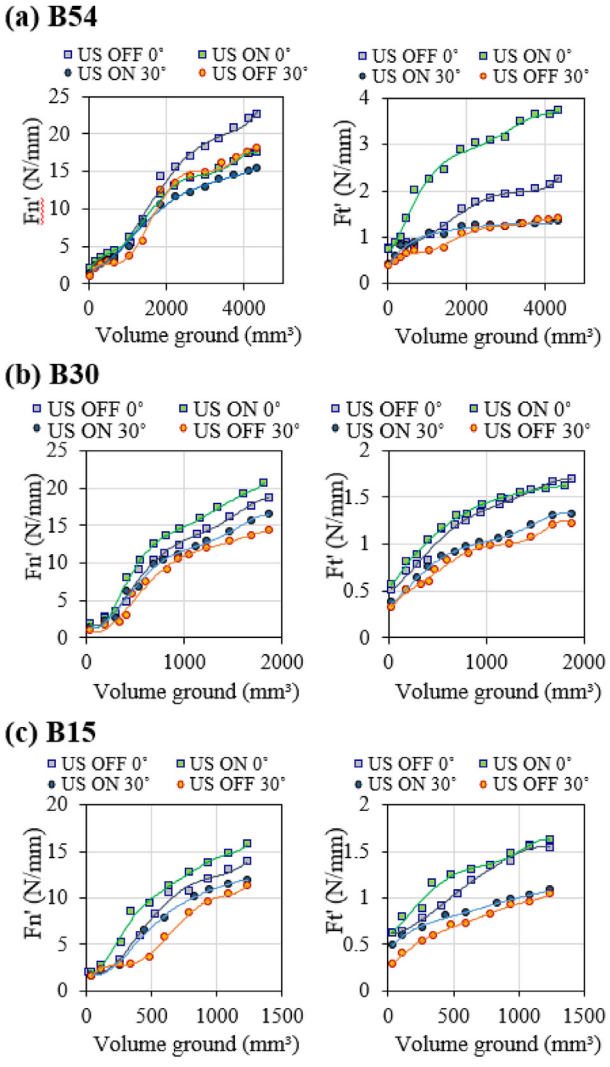

Fig. 8. Specific grinding force components under various test conditions for the: (a) B54; (b) B30; (c) B15 grinding points.

3.4. Workpiece surface finish

Representative optical micrographs and contour plots of the workpiece surfaces at test cessation for the various process configurations ground using the B15 wheels are shown in Fig. 9. When conventional grinding (US OFF) at 0° tilt, the surfaces exhibited long and distinctly linear grooves aligned to the cutting speed (v_c) direction. Likewise, operating with the workpiece inclined resulted in cutting tracks orientated parallel to the tilt angle (30°), however the scratches formed were instead needle shaped and discontinuous. Schematic diagrams illustrating the effect of workpiece angle on grind mark/scratch profiles formed for a column of grits (colour coded and numbered) are presented in Fig. 10. With the workpiece slanted at 30° relative to the tool, the cutting tracks were generated by the successive action of multiple grains at varying axial positions of the grinding point as it feeds laterally across the machined surface, see Fig. 10b. This was found to increase the distance between adjacent scratches, thereby minimising overlaps typically seen in grooves produced when machining without workpiece inclination [13]. The grind marks/tracks became less distinct in trials involving ultrasonic assistance, as the high frequency oscillations along the tool axis caused 'smearing' of the surface leading to a wave like texture, see Fig. 11. Similar results/trends were observed in tests employing the B54 and B30 wheels.

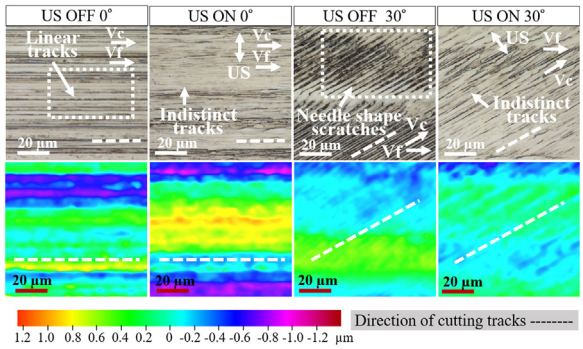

Fig. 9. Micrographs and contour plots of workpiece surfaces machined with B15 grinding points at test cessation.

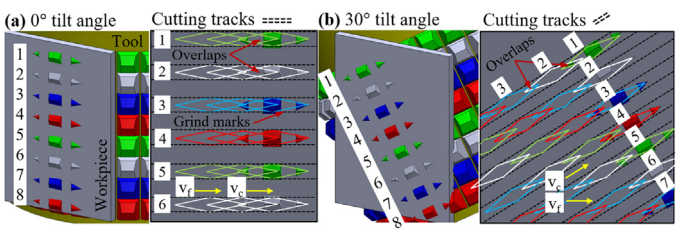

Fig. 10. Schematic diagrams showing formation of grind mark/scratch profiles at: (a) 0°; (b) 30° workpiece tilt angles.

Please cite this article as: F. Medina Aguirre et al., Assessment of advanced process configurations for improving workpiece surface finish in point grinding, CIRP Annals - Manufacturing Technology (2023), https://doi.org/10.1016/j.cirp.2023.04.078

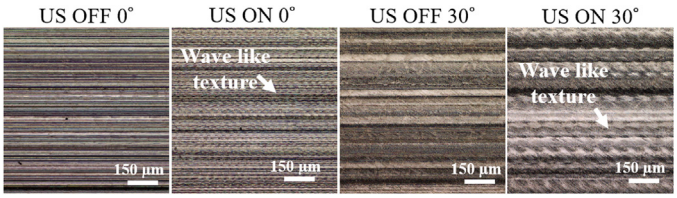

Fig. 11. Sample micrographs of workpiece surface texture following grinding using B54 tools.

Average workpiece surface roughness (Ra and Rz) measured in relation to volume ground for each of the grinding points are detailed in Fig. 12. In general, the surface roughness curves initially demonstrated a progressively decreasing trend (due to conditioning of the grits) before starting to plateau towards a steady state after ~500 mm^3 of material ground. Increasing workpiece inclination was revealed to be more significant than tool ultrasonic vibration in reducing surface roughness, with all trials at 30° tilt angle producing lower Ra/Rz values of up to ~44%/51% compared to those undertaken at 0° orientation. As the directions of v_c and v_f are not coincident when machining with the workpiece inclined, the grain trajectories are governed by the resultant displacements due to both parameters [11]. Here, the dimensions of grit marks along the v_c direction were wider due to the additional movement caused by feed motion of the tool, see Fig. 9. The increase in the width of the cutting tracks (perpendicular to v_c direction) results in a smoother transition between adjacent grooves, thereby lowering the surface roughness. Additionally, the interaction of adjacent grits along the tool axis in the cutting tracks (see Fig. 10) could have further reduced surface roughness due to greater overlays of the abrasive scratches. However, it was previously reported by Uhlmann et al. [11] that changes/improvement in workpiece surface roughness was marginal at workpiece tilt angles above 30°.

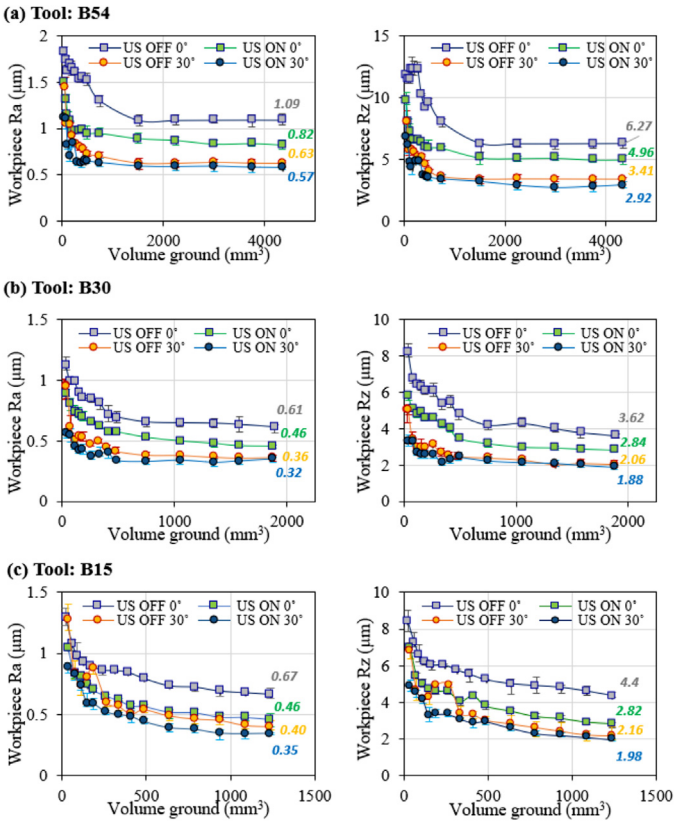

Fig. 12. Progression of workpiece surface roughness with respect to volume ground for: (a) B54; (b) B30; (c) B15 tools.

Experiments incorporating UVAG with workpieces horizontal led to a ~25% mean reduction in Ra/Rz over conventional grinding, whereas a lower average drop of ~11% was recorded when workpieces were orientated at 30°. The action of ultrasonic tool oscillations served to flatten the peaks of roughness profiles, which appeared to be more effective on surfaces ground at 0° tilt having initially higher roughness levels. The roughness achieved by the B30 and B15 tools were largely comparable due to their similar average equivalent grit size and mean grain protrusion, with lowest values approaching ~0.3 µm Ra when utilising UVAG at 30° tilt angle. This was ~44% lower than the corresponding roughness (0.57 µm Ra) attained when grinding with B54 tools.

3.5. Microhardness

Depth profile microhardness plots measured on cross sectioned samples taken parallel and perpendicular to the feed direction after a volume of material removed (VMR) of 488 mm^3 (65 passes) when workpiece surface roughness began to stabilise (see Fig. 12)/tools were conditioned, and at test cessation following trials using the B15 and B54 tools are presented in Figs. 13 and 14 respectively. All of the results indicated that no major changes in subsurface microhardness were detected in any of the workpieces except for the sample ground at 0° inclination using the B54 wheels without US vibration. Here, an increase of ~50 $HK_{0.05}$ above the bulk hardness was recorded perpendicular to the feed direction at test cessation, which extended to a depth of ~100 µm below the machined surface. This can be attributed to possible strain hardening induced by the correspondingly higher normal grinding forces generated as shown in Fig. 8a.

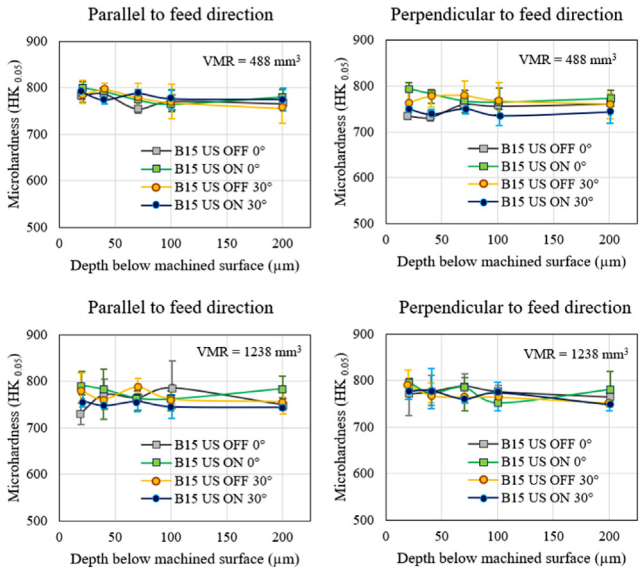

Fig. 13. Microhardness depth profiles of surfaces ground with B15 wheels sectioned parallel and perpendicular to feed direction at VMR of 488 mm^3 and test cessation.

4. Conclusions

Surface topographical assessment of the grinding points revealed that new/as supplied B15 and B30 wheels possessed similar abrasive geometrical characteristics including average grit diameter (~23 µm) and mean grain protrusion (~8–9 µm) as well as specific grit volumes (~155 × 10^4 µm^3/mm^2), which did not correspond to the manufacturer's specifications. This indicates that inspection of tools prior to use is recommended, particularly in applications where the workpiece surface finish requirements/tolerances are critical. In terms of process configuration, variation in workpiece tilt angle from 0°to 30° had the strongest effect in reducing machined surface roughness (Ra) by up to ~44%. This was largely due to the change in grit trajectory as the tools were inclined relative to the workpiece, which consequently altered the grind mark/scratch profiles and resulting surface texture/contours. In general, workpiece inclination had marginal influence on tool wear/volumetric grit loss and overall normal grinding forces. The use of ultrasonic assisted grinding operation further reduced surface roughness by 11–25%, depending on workpiece orientation.

Please cite this article as: F. Medina Aguirre et al., Assessment of advanced process configurations for improving workpiece surface finish in point grinding, CIRP Annals - Manufacturing Technology (2023), https://doi.org/10.1016/j.cirp.2023.04.078

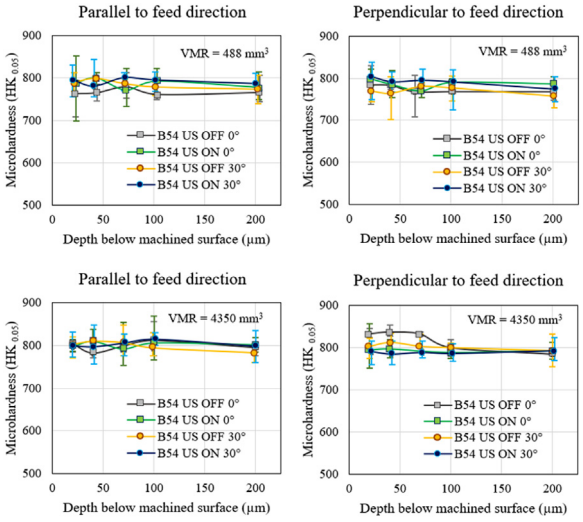

Fig. 14. Microhardness depth profiles of surfaces ground with B54 wheels sectioned parallel and perpendicular to feed direction at VMR of 488 mm^3 and test cessation.

However, grinding with ultrasonic vibration was shown to intensify volumetric grit loss of the B30 and B15 wheels as well as increase specific normal grinding forces (~14%). In contrast, wear of the B54 grinding points were approximately equivalent when machining with and without ultrasonic actuation, despite the former exhibiting lower specific normal forces (~20%). Apart from one exception, none of the ground surfaces assessed showed any significant subsurface microhardness alterations even at test cessation (both parallel and perpendicular to feed direction). This suggests that workpiece surface integrity issues relating to thermal softening or strain hardening to a large extent, did not arise under the process conditions/configurations utilised for finish point grinding of hardened steel.

Declaration of Competing Interest

The authors declare that they have no known competing financial interests or personal relationships that could have appeared to influence the work reported in this paper.

Acknowledgements

The authors are grateful for financial and technical support from Rolls-Royce plc and to the University of Birmingham for awarding scholarships to Drs. Medina Aguirre and Soriano Gonzalez.

References

[1] Curtis D, Soo SL, Aspinwall DK, Mantle AL (2016) Evaluation of Workpiece Surface Integrity Following Point Grinding of Advanced Titanium and Nickel Based Superalloys. *Procedia CIRP* 45:47–50.
[2] Pietrow N, Curtis D, Ghadbeigi H, Novovic D, McGourlay J (2021) An Investigation into the Challenges of the Point Grinding Machining Process. *Procedia CIRP* 101:190–193.
[3] Guo C, Ranganath S, McIntosh D, Elfizy A (2008) Virtual high performance grinding with CBN wheels. *CIRP Annals-Manufacturing Technology* 57(1):325–328.
[4] Hood R, Medina Aguirre F, Soriano Gonzalez L, Novovic D, Soo SL (2019) Evaluation of Superabrasive Grinding Points for the Machining of Hardened Steel. *CIRP Annals – Manufacturing Technology* 68(1):329–332.
[5] Burrows JM, Dewes RC, Aspinwall DK (2000) Grinding of Inconel 718 and Udimet 720 Using Superabrasive Grinding Points Mounted on a High Speed Machining Centre. In: *Proceedings of the 33rdInternational MATADOR Conference*, Manchester, UK447–452.
[6] Burrows JM, Dewes RC, Aspinwall DK (2002) Use of a High Speed Machining Centre for the CBN and Diamond Grinding of Nickel-Based Superalloys. in Dudzinski D, Molinari A, Schulz H, (Eds.) *Metal Cutting and High Speed Machining*, Kluwer Academic/Plenum Publishers, New York, 267–275.
[7] Dewes R, Aspinwall D, Burrows J, Paul M, El-Menshawy F (2001) High Speed Machining – Multi-Function/Hybrid Systems. In: *Proceedings of the Fourth International Conference on Industrial Tooling*, Southampton, UK91–100.
[8] Soo SL, Ng EG, Dewes RC, Aspinwall DK, Burrows JM (2002) Point Grinding of Nickel-Based Superalloys. *Industrial Diamond Review* 62(2):109–116.
[9] Aspinwall DK, Soo SL, Curtis DT, Mantle AL (2007) Profiled Superabrasive Grinding Wheels for the Machining of a Nickel Based Superalloy. *CIRP Annals-Manufacturing Technology* 56(1):335–338.
[10] Yan QS, Zhang ZQ, Syoji K (2003) Machining Precision in the Face Grinding of a Groove Bottom Using a Cup CBN Quill. *Journal of Materials Processing Technology* 138(1–3):527–530.
[11] Uhlmann E, Borsoi Klein T, Koprowski S (2014) Tilt Angle Effects in Surface Grinding with Mounted Points. *Production Engineering* 8(4):431–442.
[12] Pietrow N, Curtis D, Novovic D, McGourlay J, Ghadbeigi H (2022) Evolution of Electroplated Cubic Boron Nitride Tool Surface Texture Parameters During Point Grinding. *Transactions of the ASME - Journal of Manufacturing Science and Engineering* 144(12):121007. -1-121007-14.
[13] Zhang B (1999) Helical Scan Grinding of Brittle and Ductile Materials. *Journal of Materials Processing Technology* 91(1–3):196–205.